

Magnetic excitations in L-edge resonant inelastic x-ray scattering from one-dimensional cuprates

Jun-ichi Igarashi

Faculty of Science, Ibaraki University, Mito, Ibaraki 310-8512, Japan

Tatsuya Nagao

Faculty of Engineering, Gunma University, Kiryu, Gunma 376-8515, Japan

(Dated: November 23, 2011)

Abstract

We study the magnetic excitation spectra of L -edge resonant inelastic x-ray scattering (RIXS) from the spin singlet ground state in one-dimensional undoped cuprates. Analyzing the transition amplitudes of the magnetic excitations in the second-order dipole allowed process, we find that the magnetic excitations are brought about not only on the core-hole site but also on the neighboring sites. The RIXS spectra are expressed by the one-spin correlation function in the scattering channel with changing polarization, and the two-spin correlation function in the scattering channel without changing polarization. The latter could not be brought about within the so-called UCL approximation. We calculate these correlation functions on a finite-size ring. An application to the possible RIXS spectra in Sr_2CuO_3 demonstrates that the contribution of the two-spin correlation function could be larger than that of the one-spin correlation function in the σ polarization for the momentum transfer around the zone center.

PACS numbers: 78.70.Ck, 72.10.Di, 78.20.Bh, 74.72.Cj

I. INTRODUCTION

Resonant inelastic x-ray scattering (RIXS) has attracted much interest as a useful tool to investigate excited states in solids. Both the K -edge and the L -edge resonances are available in transition-metal compounds. To observe the momentum dependence of the spectra, it is suitable to use the K -edge resonance that the $1s$ -core electron is prompted to an empty $4p$ state by absorbing photon and then the photo-excited $4p$ electron is recombined with the core hole by emitting photon. It is known that the intensities for energy loss ω above several eV's arise from charge excitations to screen the core-hole potential.¹⁻¹⁴ A useful formalism has been developed¹⁰⁻¹² on the basis of the Keldysh Green function,¹⁵ in which the RIXS spectra are described in terms of the $3d$ -density-density correlation function. The spectra have been calculated for undoped cuprates,¹⁰⁻¹² NiO,¹⁶ and LaMnO₃,¹⁷ in good agreement with the experiments. In addition to such spectra, the intensities for ω below 1 eV have been observed from the K -edge RIXS in La₂CuO₄.^{18,19} Their origin is attributed to the magnetic excitations caused by the modification of the exchange coupling under the presence of the core-hole potential.^{20,21} The above-mentioned formalism has been adapted to describe such magnetic excitations, having led to the expression that the RIXS spectra are proportional to the two-spin correlation function, which has been evaluated by the $1/S$ -expansion method.²²

Recently, the L -edge RIXS experiments with high resolutions have been carried out in transition-metal compounds. The observed spectra for ω around several hundreds meV's can be understood as coming from magnetic excitations.²³⁻²⁵ The L -edge resonance in the undoped cuprates is described by the process that the $2p$ -core electron is prompted to the empty $x^2 - y^2$ orbital by absorbing photon, and then an occupied $3d$ electron combines with the core hole by emitting photon. If the $3d$ orbital in the photo-emitting process is different from the one in the photo-absorbing process, the excitations within the $3d$ states are brought about ("d-d" excitation).²⁶ Even if the $3d$ orbitals in the photo-absorbing and photo-emitting processes are the same, purely magnetic excitations could be generated when the direction of the staggered moment deviates from the z direction.²⁷ The spectra observed as a function of energy loss exhibit a systematic variation with changing momentum transfer.²⁵ That is, the peak position moves according to the spin-wave dispersion curve, while their shapes exhibit structures indicative of two- or three-magnon excitations.

In our previous paper,²⁸ we have analyzed the process generating the final states in

the second-order dipole allowed process, and have clarified how the spin-flip excitations are brought about on the core-hole site. We have also found that the spin-conserving excitations are brought about around the core-hole site due to the strong perturbation working in the intermediate state. Note that, within the conventional approach called UCL approximation,²⁷ no spin-conserving excitation is possible, and the spin-flip excitation is generated just on the core-hole site. Since no core hole exists in the final state, these excitations are freely moving in crystal. We have treated the quantum fluctuation in the final state within the $1/S$ expansion method, which is known to work well in the two-dimensional $S = 1/2$ Heisenberg antiferromagnet.²⁹ On the basis of these results, we have analyzed the RIXS spectra in $\text{Sr}_2\text{CuO}_2\text{Cl}_2$. The result shows that substantial intensities are generated in the high energy side of the one-magnon peak, which are originated from two- and three-magnon excitations, in good agreement with the experiment.²⁵

The above analysis has been carried out in the antiferromagnetic ordered state. Although the spin-flip excitations are likely to extend on neighboring sites due to the second-order process, the systematic analysis of such effects is quite difficult there, because the spherical symmetry is broken in the spin space. On the other hand, in the one-dimensional Heisenberg antiferromagnet, since the ground state is the spin singlet, the spherical symmetry remains intact in the spin space. Such a system is quite suitable to study how the spin excitations are generated around the core-hole site. The purpose of this paper is to clarify the nature of the magnetic excitations in RIXS by studying the spectra on the one-dimensional system. We analyze the second-order process on a microscopic model, with distinguishing the spin-flip and spin-conserving excitations. As a result, the RIXS spectra are expressed by the one-spin and two-spin correlation functions in the scattering channels with and without changing polarization, respectively. Note that the former includes the effect of the magnetic excitations generated on the neighboring sites. We could evaluate convincingly the amplitudes leading to these correlation functions on a finite-size ring. The amplitudes of the excitations on the neighboring sites are found to increase with decreasing values of the life-time broadening width of the core hole. The present analysis contrasts with the previous analysis by Haverkort,³⁰ where the form of the magnetic excitations is inferred from Hannon's formula³¹ of the resonant elastic scattering. The analysis as well as the UCL approximation applied to the one-dimensional system³² could not describe the extended nature of the excitations. Finally we analyze possible RIXS spectra in Sr_2CuO_3 , demonstrating that the contribution

of the two-spin correlation function becomes larger than that of the one-spin correlation function in the σ polarization, and could be distinguished by comparing the spectral shape as a function of energy loss between in the σ and π polarizations.

The present paper is organized as follows. In Sec. II, we describe the Hamiltonian responsible for magnetic excitations and transition-matrix elements relevant to the $L_{2,3}$ edges in cuprate compounds. We analyze the second-order process giving rise to the magnetic excitations through the intermediate state, and express the RIXS spectra in terms of spin-correlation functions. The amplitudes leading to the spin-correlation functions are evaluated on a finite-size ring. In Sec. III, we numerically calculate the spectra on a finite-size chain. Section IV is devoted to the concluding remarks. In Appendix, the $L_{2,3}$ -edge absorption coefficient is briefly discussed.

II. FORMULATION OF RIXS SPECTRA AT THE $L_{2,3}$ -EDGE

A. Second-order dipole allowed process

Aiming at the application to the one-dimensional cuprates such as Sr_2CuO_3 and SrCuO_2 , we consider each Cu atom has one hole in the $x^2 - y^2$ orbital at the half-filling, where the x and y axes are defined along the Cu-O bonds and the z along the crystal c axis. The low-energy spin excitations are described by the one-dimensional antiferromagnetic Heisenberg Hamiltonian,

$$H_{\text{mag}} = J \sum_{\langle i,j \rangle} \mathbf{S}_i \cdot \mathbf{S}_j, \quad (2.1)$$

with $S = 1/2$ and $J > 0$. The ground state is known to be the spin singlet due to the quantum fluctuation. Unlike the antiferromagnetic ordered state, the spin singlet state possesses no special direction in the spin space. To manifest the rotational invariance in the spin space, we define the spin coordinate frame of x', y', z' axes by rotating the crystal-fixed coordinate frame of a, b, c axes with the Euler angles α, β , and γ .

In the electric dipole ($E1$) transition, a $2p$ -core electron is excited to the $3d$ states at the transition-metal $L_{2,3}$ -edge. The $2p$ states are characterized by the total angular momentum $j = 3/2$ and $1/2$ due to the strong spin-orbit interaction. The eigenstates with $j = 3/2$ may be expressed as $|\phi_1 \uparrow\rangle, \sqrt{1/3}|\phi_1 \downarrow\rangle + \sqrt{2/3}|\phi_0 \uparrow\rangle, \sqrt{2/3}|\phi_0 \downarrow\rangle + \sqrt{1/3}|\phi_{-1} \uparrow\rangle, |\phi_{-1} \downarrow\rangle$, for $m = 3/2, 1/2, -1/2, -3/2$, respectively, and those with $j = 1/2$ may be expressed

as $-\sqrt{2/3}|\phi_1 \downarrow\rangle + \sqrt{1/3}|\phi_0 \uparrow\rangle$, $-\sqrt{1/3}|\phi_0 \downarrow\rangle + \sqrt{2/3}|\phi_{-1} \uparrow\rangle$, for $m = 1/2$ and $-1/2$, respectively, where m represents the magnetic quantum number. The orbitals ϕ_1 , ϕ_0 , and ϕ_{-1} have the same angular dependence as the spherical harmonics Y_{11} , Y_{10} and Y_{1-1} , respectively. The coordinate frame for both orbital and spin of the core hole is fixed to the crystal, which is different from that for the spins of the $3d$ states, that is, \uparrow and \downarrow are associated with the direction of the crystal c axis. The corresponding interaction between photon and electron at site i may be described as

$$H_{\text{int}} = w \sum_{\mathbf{q}, \mu} \frac{1}{\sqrt{2\omega_{\mathbf{q}}}} \sum_{i, m, \sigma} D^{\mu}(jm, \sigma) h_{jm}^{\dagger} c_{\mathbf{q}\mu} d_{i\sigma} e^{i\mathbf{q} \cdot \mathbf{r}_i} + \text{H.c.}, \quad (2.2)$$

where $c_{\mathbf{q}\mu}$ stands for the annihilation operator of photon with momentum \mathbf{q} and polarization μ . The h_{jm}^{\dagger} represents the creation operator of the $2p$ hole with jm , and $d_{i\sigma}$ denotes the annihilation operator of the $3d$ hole with the $x^2 - y^2$ orbital and spin σ . The w is a constant proportional to $\int_0^{\infty} r^3 R_{3d}(r) R_{2p}(r) dr$ where $R_{3d}(r)$ and $R_{2p}(r)$ are the radial wave-functions for the $3d$ and $2p$ states of Cu atom. The $D^{\mu}(jm, \sigma)$ describes the dependence on the core-hole state and $3d$ spin, which is shown in Table I of Ref. 28.

With this interaction, the RIXS spectra may be expressed by the second-order dipole allowed process:

$$W(q_f \alpha_f; q_i \alpha_i) = 2\pi \sum_{f'} \left| \sum_n \frac{\langle \Phi_{f'} | H_{\text{int}} | n \rangle \langle n | H_{\text{int}} | \Phi_i \rangle}{E_g + \omega_i - E_n} \right|^2 \times \delta(E_g + \omega_i - E_{f'} - \omega_f), \quad (2.3)$$

with $q_i \equiv (\mathbf{q}_i, \omega_i)$, $q_f \equiv (\mathbf{q}_f, \omega_f)$, $|\Phi_i\rangle = c_{q_i \alpha_i}^{\dagger} |g\rangle$, $|\Phi_{f'}\rangle = c_{q_f \alpha_f} |f'\rangle$, where $|g\rangle$ and $|f'\rangle$ represent the ground state and excited states of the matter with energy E_g and $E_{f'}$, respectively.

B. Magnetic excitations around the core-hole site

Assuming that the core hole is created at the origin in the intermediate state, we write the ground state $|g\rangle$ of H_{mag} as

$$|g\rangle = |\uparrow\rangle |\psi_0^{\uparrow}\rangle + |\downarrow\rangle |\psi_0^{\downarrow}\rangle, \quad (2.4)$$

where $|\uparrow\rangle$ and $|\downarrow\rangle$ represent the spin states at the origin, and $|\psi_0^{\uparrow}\rangle$ and $|\psi_0^{\downarrow}\rangle$ are constructed by the bases of the rest of spins.

Then, just after the $E1$ transition, the wave function may be written as

$$H_{\text{int}}|g\rangle \propto \sum_m \left[\sum_{\sigma=\uparrow,\downarrow} D^{\alpha_i}(jm, \sigma) |\psi_0^\sigma\rangle \right] |jm\rangle, \quad (2.5)$$

where $|jm\rangle$ represents the core hole state. Note that the spin degree of freedom is lost at the origin in the intermediate state.

Let H' be the Hamiltonian in the intermediate state. The states $|\psi_0^\uparrow\rangle$ and $|\psi_0^\downarrow\rangle$ are not the eigenstates of H' . Introducing the normalized eigenstate $|\phi_\eta\rangle$'s of H' with eigenvalue ϵ'_η , we rewrite the second-order optical process as

$$\begin{aligned} & \sum_n H_{\text{int}}|n\rangle \frac{1}{\omega_i + E_g - E_n} \langle n|H_{\text{int}}|g\rangle \\ & \propto \sum_{m,\sigma,\sigma'} D^{\alpha_f}(jm, \sigma)^* D^{\alpha_i}(jm, \sigma') \\ & \quad \times \sum_\eta |\sigma\rangle |\phi_\eta\rangle R(\epsilon'_\eta) \langle \phi_\eta | \psi_0^{\sigma'} \rangle, \end{aligned} \quad (2.6)$$

with

$$R(\epsilon'_\eta) = \frac{1}{\omega_i + \epsilon_g - \epsilon_{\text{core}} + i\Gamma - \epsilon'_\eta}, \quad (2.7)$$

where ϵ_g represents the ground state energy of H_{mag} . The ϵ_{core} denotes the energy required to create a core hole in the state $|jm\rangle$ and the $3d^{10}$ -configuration. The Γ stands for the life-time broadening width of the core hole; $\Gamma \sim 0.3$ eV at the Cu L_3 edge. We write the polarization-dependent factor by

$$\sum_m D^{\alpha_f}(jm, \sigma)^* D^{\alpha_i}(jm, \sigma) \equiv P_\sigma^{(0)}(j; \alpha_f, \alpha_i), \quad (2.8)$$

$$\sum_m D^{\alpha_f}(jm, \sigma)^* D^{\alpha_i}(jm, -\sigma) \equiv P_\sigma^{(1)}(j; \alpha_f, \alpha_i). \quad (2.9)$$

Table I shows $P_\sigma^{(0)}$ and $P_\sigma^{(1)}$ for α_i and α_f along the x , y , and z axes, where $\text{sgn}(\sigma) = 1$ for $\sigma = \uparrow$ and -1 for $\sigma = \downarrow$.

1. Scattering channel with changing polarization

We analyze the scattering channel that changes the polarization during the process at the L_3 -edge. Let α_i and α_f be along y and x axes, respectively. We have the spin-conserving

TABLE I: $P_\sigma^{(0)}(j; \alpha_f, \alpha_i)$ and $P_\sigma^{(1)}(j; \alpha_f, \alpha_i)$ where upper and lower signs correspond to $\sigma = \uparrow$ and \downarrow , respectively.

		$P_\sigma^{(0)}$			$P_\sigma^{(1)}$		
j	$\alpha_f \setminus \alpha_i$	x	y	z	x	y	z
$\frac{3}{2}$	x	$\frac{2}{15}$	$\mp \frac{i}{15} \cos \beta$	0	0	$\frac{i}{15} e^{\pm i\gamma} \sin \beta$	0
	y	$\pm \frac{i}{15} \cos \beta$	$\frac{2}{15}$	0	$-\frac{i}{15} e^{\pm i\gamma} \sin \beta$	0	0
	z	0	0	0	0	0	0
$\frac{1}{2}$	x	$\frac{1}{15}$	$\pm \frac{i}{15} \cos \beta$	0	0	$-\frac{i}{15} e^{\pm i\gamma} \sin \beta$	0
	y	$\mp \frac{i}{15} \cos \beta$	$\frac{1}{15}$	0	$\frac{i}{15} e^{\pm i\gamma} \sin \beta$	0	0
	z	0	0	0	0	0	0

term coming from $P_\sigma^{(0)}$ and the spin-flipping term coming from $P_\sigma^{(1)}$. The spin-conserving term is given by

$$\begin{aligned}
& \sum_n H_{\text{int}} |n\rangle \frac{1}{\omega_i + E_g - E_n} \langle n | H_{\text{int}} | g \rangle \\
& \propto P_\uparrow^{(0)} | \uparrow \rangle \sum_\eta |\phi_\eta\rangle R(\epsilon'_\eta) \langle \phi_\eta | \psi_0^\uparrow \rangle + P_\downarrow^{(0)} | \downarrow \rangle \sum_\eta |\phi_\eta\rangle R(\epsilon'_\eta) \langle \phi_\eta | \psi_0^\downarrow \rangle, \\
& \propto \left(-\frac{i}{15} \right) \cos \beta \left\{ | \uparrow \rangle \sum_\eta |\phi_\eta\rangle R(\epsilon'_\eta) \langle \phi_\eta | \psi_0^\uparrow \rangle - | \downarrow \rangle \sum_\eta |\phi_\eta\rangle R(\epsilon'_\eta) \langle \phi_\eta | \psi_0^\downarrow \rangle \right\}. \quad (2.10)
\end{aligned}$$

We consider the states $S_0^{z'} |g\rangle$ and $(S_1^{z'} + S_{-1}^{z'}) |g\rangle$ onto which Eq. (2.10) is projected. Although they are orthogonal to $|g\rangle$, they are not orthogonal to each other nor normalized. Let $|\psi_1\rangle$ and $|\psi_2\rangle$ be $S_0^{z'} |g\rangle$ and $(S_1^{z'} + S_{-1}^{z'}) |g\rangle$, respectively. Then, the overlap matrix $(\hat{\rho}_{z'})_{i,j} \equiv \langle \psi_i | \psi_j \rangle$ is given by

$$\hat{\rho}_{z'} = \begin{pmatrix} \frac{1}{4} & 2a \\ 2a & \frac{1}{2} + 2b \end{pmatrix}, \quad (2.11)$$

where a and b are static correlation functions between the nearest and the second-nearest pairs, respectively, that is, $a = \langle S_1^{z'} S_0^{z'} \rangle = \langle S_{-1}^{z'} S_0^{z'} \rangle$, $b = \langle S_1^{z'} S_{-1}^{z'} \rangle$. Using the inverse of $\hat{\rho}_{z'}$,

we obtain

$$\begin{aligned} & \sum_n H_{\text{int}}|n\rangle \frac{1}{\omega_i + E_g - E_n} \langle n|H_{\text{int}}|g\rangle \\ & \propto \left(-\frac{i}{15}\right) \cos \beta \left\{ f_1^{(1)}(\omega_i) S_0^{z'} + f_2^{(1)}(\omega_i) (S_1^{z'} + S_{-1}^{z'}) \right\} |g\rangle, \end{aligned} \quad (2.12)$$

where

$$f_m^{(1)}(\omega_i) = \sum_{n=1,2} (\hat{\rho}_{z'}^{-1})_{m,n} (Q_{z'}^{(1)})_n, \quad (2.13)$$

with

$$(Q_{z'}^{(1)})_1 = \langle \psi_0^\uparrow | \sum_\eta |\phi_\eta\rangle R(\epsilon'_\eta) \langle \phi_\eta | \psi_0^\uparrow \rangle, \quad (2.14)$$

$$(Q_{z'}^{(1)})_2 = 4 \langle \psi_0^\uparrow | S_1^{z'} \sum_\eta |\phi_\eta\rangle R(\epsilon'_\eta) \langle \phi_\eta | \psi_0^\uparrow \rangle. \quad (2.15)$$

Therefore, the final state is expressed as

$$\begin{aligned} & \left(-\frac{i}{15}\right) \cos \beta \left[f_1^{(1)}(\omega_i) S_0^{z'} + f_2^{(1)}(\omega_i) (S_1^{z'} + S_{-1}^{z'}) \right] |g\rangle \\ & = \left(-\frac{i}{15}\right) \boldsymbol{\alpha}_{f\perp} \times \boldsymbol{\alpha}_{i\perp} \cdot \left[f_1^{(1)}(\omega_i) \mathbf{S}_{0\parallel} + f_2^{(1)}(\omega_i) (\mathbf{S}_{1\parallel} + \mathbf{S}_{-1\parallel}) \right] |g\rangle \end{aligned} \quad (2.16)$$

where $\mathbf{S}_{j\parallel}$ stands for the z' component of \mathbf{S}_j . The $\boldsymbol{\alpha}_{i\perp}$ and $\boldsymbol{\alpha}_{f\perp}$ represent the polarization vectors projected onto the x - y plane. Therefore $\boldsymbol{\alpha}_{f\perp} \times \boldsymbol{\alpha}_{i\perp}$ is always parallel to the z axis.

The spin-flip term may be expressed as

$$\begin{aligned} & \sum_n H_{\text{int}}|n\rangle \frac{1}{\omega_i + E_g - E_n} \langle n|H_{\text{int}}|g\rangle \\ & \propto P_{\downarrow}^{(1)} |\downarrow\rangle \sum_\eta |\phi_\eta\rangle R(\epsilon'_\eta) \langle \phi_\eta | \psi_0^\uparrow \rangle + P_{\uparrow}^{(1)} |\uparrow\rangle \sum_\eta |\phi_\eta\rangle R(\epsilon'_\eta) \langle \phi_\eta | \psi_0^\downarrow \rangle, \\ & \propto \left(\frac{i}{15}\right) \sin \beta \left\{ e^{-i\gamma} |\downarrow\rangle \sum_\eta |\phi_\eta\rangle R(\epsilon'_\eta) \langle \phi_\eta | \psi_0^\uparrow \rangle + e^{i\gamma} |\uparrow\rangle \sum_\eta |\phi_\eta\rangle R(\epsilon'_\eta) \langle \phi_\eta | \psi_0^\downarrow \rangle \right\}. \end{aligned} \quad (2.17)$$

We project this state onto a pair of states $S_0^+|g\rangle$ and $(S_1^+ + S_{-1}^+)|g\rangle$, and another pair of states $S_0^-|g\rangle$ and $(S_1^- + S_{-1}^-)|g\rangle$, where $S_j^\pm = S_j^{x'} \pm iS_j^{y'}$. The states belonging to different pairs are orthogonal. Defining the overlap matrices $\hat{\rho}_+$ and $\hat{\rho}_-$ for each pair in a similar way used for $\hat{\rho}_{z'}$, we immediately notice that

$$\hat{\rho}_+ = \hat{\rho}_- = 2\hat{\rho}_{z'}. \quad (2.18)$$

The second term of Eq. (2.17) is projected onto the first pair of the states, leading to

$$\propto \left(\frac{i}{15}\right) \sin \beta e^{i\gamma} \{g_1(\omega_i)S_0^+ + g_2(\omega_i)(S_1^+ + S_{-1}^+)\} |g\rangle, \quad (2.19)$$

where

$$g_m(\omega_i) = \sum_{n=1,2} (\hat{\rho}_+^{-1})_{m,n} (Q_+^{(1)})_n, \quad (2.20)$$

with

$$(Q_+^{(1)})_1 = \langle \psi_0^\dagger | \sum_{\eta} |\phi_{\eta}\rangle R(\epsilon'_{\eta}) \langle \phi_{\eta} | \psi_0^\dagger \rangle = (Q_z^{(1)})_1, \quad (2.21)$$

$$(Q_+^{(1)})_2 = 2\langle \psi_0^\dagger | S_1^- \sum_{\eta} |\phi_{\eta}\rangle R(\epsilon'_{\eta}) \langle \phi_{\eta} | \psi_0^\dagger \rangle = (Q_z^{(1)})_2. \quad (2.22)$$

Hence we have $g_1(\omega_i) = (1/2)f_1^{(1)}(\omega_i)$ and $g_2(\omega_i) = (1/2)f_2^{(1)}(\omega_i)$. The similar relations are obtained for the first term of Eq. (2.17) by using the second pair of the states. Therefore Eq. (2.17) is expressed as

$$\begin{aligned} & \propto \left(\frac{i}{15}\right) \sin \beta \left\{ \cos \gamma [f_1^{(1)}(\omega_i)S_0^{x'} + f_2^{(1)}(\omega_i)(S_1^{x'} + S_{-1}^{x'})] \right. \\ & \quad \left. - \sin \gamma [f_1^{(1)}(\omega_i)S_0^{y'} + f_2^{(1)}(\omega_i)(S_1^{y'} + S_{-1}^{y'})] \right\} |g\rangle \\ & = \left(-\frac{i}{15}\right) \boldsymbol{\alpha}_{f\perp} \times \boldsymbol{\alpha}_{i\perp} \cdot [f_1^{(1)}(\omega_i)\mathbf{S}_{0\perp} + f_2^{(1)}(\omega_i)(\mathbf{S}_{1\perp} + \mathbf{S}_{-1\perp})] |g\rangle, \end{aligned} \quad (2.23)$$

where $\mathbf{S}_{j\perp}$ stands for the component perpendicular to the z' axis of \mathbf{S}_j . Combining this result with Eq. (2.16), we finally obtain

$$\begin{aligned} & \sum_n H_{\text{int}} |n\rangle \frac{1}{\omega_i + E_g - E_n} \langle n | H_{\text{int}} | g \rangle \\ & = \left(-\frac{i}{15}\right) \boldsymbol{\alpha}_f \times \boldsymbol{\alpha}_i \cdot [f_1^{(1)}(\omega_i)\mathbf{S}_0 + f_2^{(1)}(\omega_i)(\mathbf{S}_1 + \mathbf{S}_{-1})] |g\rangle. \end{aligned} \quad (2.24)$$

Excitations on further neighboring sites are included by adding a term $f_3^{(1)}(\omega_i)(\mathbf{S}_2 + \mathbf{S}_{-2})|g\rangle$ with $f_3^{(1)}(\omega_i)$ similarly determined coefficient.

Collecting up the amplitudes from all sites, we obtain the expression of the RIXS spectra for the polarizations $\boldsymbol{\alpha}_{i(f)} = (\alpha_{i(f)}^x, \alpha_{i(f)}^y, \alpha_{i(f)}^z)$,

$$W(q_f, \omega_f, \alpha_f; q_i, \omega_i, \alpha_i) = \frac{w^4}{4\omega_i\omega_f} \left(\frac{1}{15}\right)^2 (\alpha_f^x \alpha_i^y - \alpha_f^y \alpha_i^x)^2 Y^{(1)}(\omega_i; q, \omega), \quad (2.25)$$

where

$$Y^{(1)}(\omega_i; q, \omega) = \int \langle Z^{(1)\dagger}(\omega_i; q, t) Z^{(1)}(\omega_i; q, 0) \rangle e^{i\omega t} dt, \quad (2.26)$$

with

$$\begin{aligned}
Z^{(1)}(\omega_i; q) &= \sum_j [f_1^{(1)}(\omega_i)S_j^z + f_2^{(1)}(\omega_i)(S_{j+1}^z + S_{j-1}^z) + f_3^{(1)}(\omega_i)(S_{j+2}^z + S_{j-2}^z)]e^{-iqr_j} \\
&= [f_1^{(1)}(\omega_i) + 2f_2^{(1)}(\omega_i)\cos q + 2f_3^{(1)}(\omega_i)\cos(2q)] \sum_j S_j^z e^{-iqr_j}.
\end{aligned} \tag{2.27}$$

The presence of $f_2^{(1)}(\omega_i)$ and $f_3^{(1)}(\omega_i)$ modifies the q -dependence of the spectra, but the spectral shape as a function of ω is expressed by the conventional correlation function.

2. Scattering channel without changing polarization

In this scattering channel, only the spin-conserving excitations are brought about through the diagonal components of $P_\sigma^{(0)}$. For each component, we have

$$\begin{aligned}
&\sum_n H_{\text{int}}|n\rangle \frac{1}{\omega_i + E_g - E_n} \langle n|H_{\text{int}}|g\rangle \\
&\propto \left(\frac{2}{15}\right) \left\{ |\uparrow\rangle \sum_\eta |\phi_\eta\rangle R(\epsilon'_\eta) \langle \phi_\eta|\psi_0^\uparrow\rangle + |\downarrow\rangle \sum_\eta |\phi_\eta\rangle R(\epsilon'_\eta) \langle \phi_\eta|\psi_0^\downarrow\rangle \right\}.
\end{aligned} \tag{2.28}$$

Since the polarization dependence behaves as $\boldsymbol{\alpha}_{f\perp} \cdot \boldsymbol{\alpha}_{i\perp}$, the corresponding spin excitations may be expressed by operating even number of spin operators on the ground state. Therefore it is reasonable to assume the excited states as $(\mathbf{S}_1 + \mathbf{S}_{-1}) \cdot \mathbf{S}_0|g\rangle$, $(\mathbf{S}_2 + \mathbf{S}_{-2}) \cdot \mathbf{S}_0|g\rangle$, and $\mathbf{S}_1 \cdot \mathbf{S}_{-1}|g\rangle$. Since these states are not orthogonal to $|g\rangle$, we define the overlap matrix $\hat{\rho}$ by including $|g\rangle$ to be projected in addition to the above three states. The procedure of projection is the same as before. Here we simply write down the result;

$$\begin{aligned}
&\sum_n H_{\text{int}}|n\rangle \frac{1}{\omega_i + E_g - E_n} \langle n|H_{\text{int}}|g\rangle \\
&\propto \frac{2}{15} \boldsymbol{\alpha}_{f\perp} \cdot \boldsymbol{\alpha}_{i\perp} \left\{ f_1^{(2)}(\omega_i) + f_2^{(2)}(\omega_i)(\mathbf{S}_1 + \mathbf{S}_{-1}) \cdot \mathbf{S}_0 \right. \\
&\quad \left. + f_3^{(2)}(\omega_i)(\mathbf{S}_2 + \mathbf{S}_{-2}) \cdot \mathbf{S}_0 + f_4^{(2)}(\omega_i)\mathbf{S}_1 \cdot \mathbf{S}_{-1} \right\} |g\rangle.
\end{aligned} \tag{2.29}$$

Collecting up the contribution from all sites, we obtain the RIXS spectra for the polarization vectors $\boldsymbol{\alpha}_i$ and $\boldsymbol{\alpha}_f$,

$$W(q_f, \omega_f, \alpha_f; q_i, \omega_i, \alpha_i) = \frac{w^4}{4\omega_i\omega_f} \left(\frac{2}{15}\right)^2 (\alpha_f^x \alpha_i^x + \alpha_f^y \alpha_i^y)^2 Y^{(2)}(\omega_i; q, \omega), \tag{2.30}$$

where

$$Y^{(2)}(\omega_i; q, \omega) = \int \langle Z^{(2)\dagger}(\omega_i; q, t) Z^{(2)}(\omega_i; q, 0) \rangle e^{i\omega t} dt, \tag{2.31}$$

with

$$Z^{(2)}(\omega_i; q) = \sum_j \left\{ f_2^{(2)}(\omega_i)(\mathbf{S}_{j+1} + \mathbf{S}_{j-1}) \cdot \mathbf{S}_j + f_3^{(2)}(\omega_i)(\mathbf{S}_{j+2} + \mathbf{S}_{j-2}) \cdot \mathbf{S}_j + f_4^{(2)}(\omega_i)\mathbf{S}_{j+1} \cdot \mathbf{S}_{j-1} \right\} e^{-iqr_j}. \quad (2.32)$$

In the far-off-resonance condition that $|\omega_i + \epsilon_g - \epsilon_{\text{core}}| \gg \Gamma, \epsilon'_\eta$, and in the UCL approximation that $\Gamma \gg |\omega_i + \epsilon_g - \epsilon_{\text{core}}|, \epsilon'_\eta$, we could factor out $R(\epsilon'_\eta)$ in Eq. (2.28). In such circumstances, using the relation $\sum_\eta |\phi_\eta\rangle\langle\phi_\eta| = 1$, we notice that Eq. (2.28) is proportional to $|g\rangle$, that is, no excitations are generated.

C. Evaluation of coefficients

For evaluating $f_\mu^{(1)}(\omega_i)$'s and $f_\nu^{(2)}(\omega_i)$'s, we consider a system consisting of 12 spins of $S = 1/2$ with periodic boundary conditions for the initial and final states, as shown in Fig. 1. Since the relevant magnetic excitations are restricted around the core-hole site, we expect that a system having rather small size works well. Representing H_{mag} by a matrix of 924×924 dimensions in the subspace of the z' component of the total spin $S_{\text{tot}}^{z'} = 0$, we diagonalize the Hamiltonian matrix. We obtain the ground state energy as $\epsilon_g/(NJ) = -0.448$, which should be compared with the exact value -0.443 .³³ On the other hand, the intermediate state is expressed by using 11 spins, since the spin degree of freedom is lost at the core-hole site. Therefore H' may be represented by a matrix with 462×462 dimensions in the subspace of $S_{\text{tot}}^{z'} = \pm 1/2$.

As briefly discussed in Appendix and shown there in Fig. 6, the absorption coefficient for the transition $2p \rightarrow 3d_{x^2-y^2}$ in cuprates has a single-peak structure; the peak is located at $\omega_i = \omega_i^0 \equiv \epsilon_{\text{core}} + 0.8J$. Note that the incident photon energy ω_i is usually tuned to give the maximum absorption coefficient in RIXS experiments. For Sr_2CuO_3 and SrCuO_2 , J is rather large (200 – 250 meV), and $\Gamma \sim 0.3$ eV, and thereby we have $\Gamma/J \sim 1.2$.

Using the eigenvalues and eigenfunctions on a ring of 12 spins, we calculate the coefficients for $\omega_i = \omega_i^0$. Table II lists the calculated values. For $f_\mu^{(1)}$'s, $|f_2^{(1)}|$ and $|f_3^{(1)}|$ are rather smaller than $|f_1^{(1)}|$ with $\Gamma/J = 1.2$, while they become larger with $\Gamma/J = 0.5$, indicating that the effect of magnetic excitations on neighboring sites increases with decreasing value of Γ . As regards $f_\nu^{(2)}$'s, $|f_2^{(2)}|$ overwhelms other absolute values even when $\Gamma/J = 0.5$. This suggests that the disturbance is nearly limited within the nearest neighbor sites.

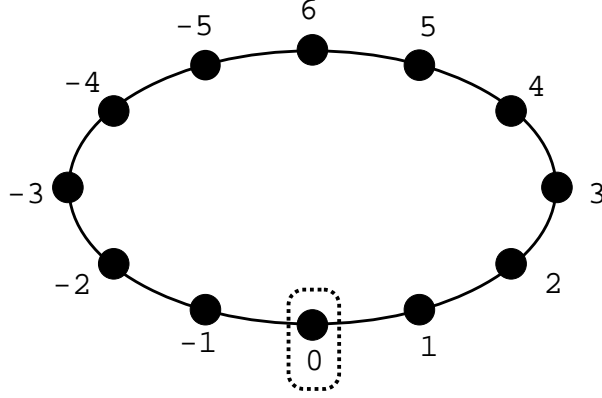


FIG. 1: A ring of 12 spins used to evaluate $f_{\mu}^{(1)}(\omega_i)$'s and $f_{\nu}^{(2)}(\omega_i)$'s. The spin at site 0 is annihilated in the intermediate state.

TABLE II: Coefficients $f_{\mu}^{(1)}(\omega_i^0)$'s and $f_{\nu}^{(1)}(\omega_i^0)$'s in units of $1/J$.

Γ/J	$f_1^{(1)}(\omega_i^0)$	$f_2^{(1)}(\omega_i^0)$	$f_3^{(1)}(\omega_i^0)$
1.2	(0.182, -1.752)	(0.282, -0.188)	(0.165, -0.106)
0.5	(0.649, -4.395)	(0.723, -0.979)	(0.426, -0.567)

Γ/J	$f_2^{(2)}(\omega_i^0)$	$f_3^{(2)}(\omega_i^0)$	$f_4^{(2)}(\omega_i^0)$
1.2	(0.038, -0.365)	(-0.007, 0.009)	(0.039, -0.067)
0.5	(-0.431, -0.543)	(0.010, 0.022)	(-0.074, -0.142)

III. RIXS SPECTRA

Since the magnetic excitations could propagate in the crystal in the final state because of the absence of core hole, a small-size ring would not work well. In the following, we calculate the correlation functions on a ring of 16 spins from Eqs. (2.26) and (2.31). Figure 2 shows $Y^{(1)}(\omega_i^0; q, \omega)$ and $Y^{(2)}(\omega_i^0; q, \omega)$ numerically calculated with $\Gamma/J = 1.2$. The blue lines represent the des Cloizeaux-Pearson curve,³⁴ $\omega = J(\pi/2) \sin q$, which is the lowest boundary of the excitation energy. These functions have already been obtained from the calculation on a finite-size system³² and also from the Bethe Ansatz solution.³⁵ The spectral shape of $Y^{(2)}(\omega_i^0; q, \omega)$ as a function of ω seems to have more weights at higher ω than that of $Y^{(1)}(\omega_i^0; q, \omega)$.

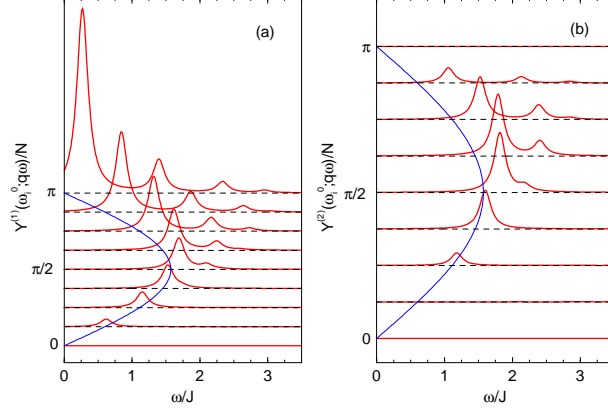


FIG. 2: (Color online) Correlation functions calculated on a ring of 16 spins, as a function of energy loss ω for various q -values; (a) $Y^{(1)}(\omega_i^0; q, \omega)/N$ and (b) $Y^{(2)}(\omega_i^0; q, \omega)/N$, with ω_i^0 the photon energy giving rise to the peak in the absorption spectra, and $\Gamma/J = 1.2$. The blue lines represent the des Cloizeaux-Pearson curve, which is the lowest boundary of the excitation energy.

Figure 3 shows the integrated intensities defined by

$$I^{(1)}(\omega_i^0; q) = \int Y^{(1)}(\omega_i^0; q, \omega) \frac{d\omega}{2\pi}, \quad (3.1)$$

$$I^{(2)}(\omega_i^0; q) = \int Y^{(2)}(\omega_i^0; q, \omega) \frac{d\omega}{2\pi}. \quad (3.2)$$

The $I^{(1)}(\omega_i^0; q)$ vanishes with $q \rightarrow 0$, increases with increasing values of q , and remains finite with $q \rightarrow \pi$. The presence of $f_2^{(1)}(\omega_i)$ and $f_3^{(1)}(\omega_i)$ makes the q -dependence deviate from that of the dynamical structure factor. The deviation becomes conspicuous with $\Gamma/J = 0.5$, because of the increase of $|f_2^{(1)}(\omega_i^0)|$ and $|f_3^{(1)}(\omega_i^0)|$. The $I^{(2)}(\omega_i^0; q)$ is found one order of magnitude smaller than $I^{(1)}(\omega_i^0; q)$ around the zone center.

Bearing in mind a possible application to Sr_2CuO_3 , we demonstrate the importance of $Y^{(2)}(\omega_i^0; q, \omega)$ by calculating the RIXS spectra on the L_3 edge under a typical scattering geometry shown in Fig. 4, the same geometry as used in the experiment in $\text{Sr}_2\text{CuO}_2\text{Cl}_2$;²⁵ the angle between the incident and the scattered x-ray is kept 130 degrees, and the scattering plane includes the $b(x)$ and $c(z)$ axes. The polarization vector of the incident photon is then expressed as $\boldsymbol{\alpha}_i = (0, -1, 0)$ for the σ polarization and $\boldsymbol{\alpha}_i = (\chi_i^\pi, 0, \tilde{\chi}_i^\pi)$ for the π polarization. Similarly, the polarization of the scattered photon is expressed as $\boldsymbol{\alpha}_f = (0, -1, 0)$ for the σ' polarization and $\boldsymbol{\alpha}_f = (\chi_f^\pi, 0, \tilde{\chi}_f^\pi)$ for the π' polarization. The polarization is usually separated with the incident photon, but not separated with the scattered photon in experiments. In such a situation, we may express the RIXS spectra depending on the polarization

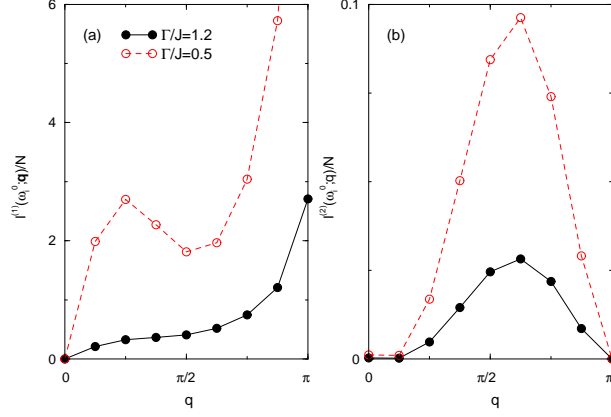


FIG. 3: (Color online) Frequency-integrated intensities of the correlation functions, (a) $I^{(1)}(\omega_i^0; q)/N$ and (b) $I^{(2)}(\omega_i^0; q)/N$, calculated on a ring of 16 spins as a function of q . The ω_i^0 is the photon energy giving rise to the peak in the absorption spectra. Filled black and open red circles correspond to $\Gamma/J = 1.2$ and 0.5 , respectively. Curves are guides to the eye.

of the incident photon as

$$I(\omega_i; q, \omega) = \frac{w^4}{4\omega_i\omega_f} \times \begin{cases} \left[\left(\frac{\chi_f^\pi}{15} \right)^2 Y^{(1)}(\omega_i; q, \omega) + \left(\frac{2}{15} \right)^2 Y^{(2)}(\omega_i; q, \omega) \right], & (\sigma - \text{pol.}), \\ \left[\left(\frac{\chi_i^\pi}{15} \right)^2 Y^{(1)}(\omega_i; q, \omega) + \left(\frac{2\chi_f^\pi\chi_i^\pi}{15} \right)^2 Y^{(2)}(\omega_i; q, \omega) \right], & (\pi - \text{pol.}), \end{cases} \quad (3.3)$$

where q is regarded as the transferred momentum projected onto the b axis. The contribution of $Y^{(2)}(\omega_i; q, \omega)$ relative to that of $Y^{(1)}(\omega_i; q, \omega)$ is enhanced by $(2/\chi_f^\pi)^2$ in the σ polarization. The contribution of $Y^{(2)}(\omega_i; q, \omega)$ in the π polarization is reduced from that in the σ polarization by a factor $(\chi_f^\pi\chi_i^\pi)^2$.

Figure 5 shows the RIXS spectrum as a function of energy loss ω for $q = 3\pi/4(-3\pi/4)$, where $\chi_i^\pi = 0.89(0.23)$, $\chi_f^\pi = 0.23(0.89)$ for $\omega_i \sim 930$ eV and $b = 3.49$ Å. We put $J \sim 260$ meV and $\Gamma/J = 1.2$. The calculated curves are convoluted by the Lorentzian function with the half-width-half-maximum of the possible resolution, 78 meV. The contribution of $Y^{(1)}(\omega_i^0; q, \omega)$ dominates the spectra in the π polarization at both $q = \pm 3\pi/4$, while the contribution of $Y^{(2)}(\omega_i; q, \omega)$ relative to that of $Y^{(1)}(\omega_i; q, \omega)$ increases in the σ polarization due to the polarization factor.

At $q = 3\pi/4$, the contribution of $Y^{(2)}(\omega_i^0; q, \omega)$ becomes even larger than that of $Y^{(1)}(\omega_i^0; q, \omega)$. Since the contribution of $Y^{(1)}(\omega_i^0; q, \omega)$ in the σ polarization could be estimated experimentally from the spectra in the π polarization by multiplying the polarization

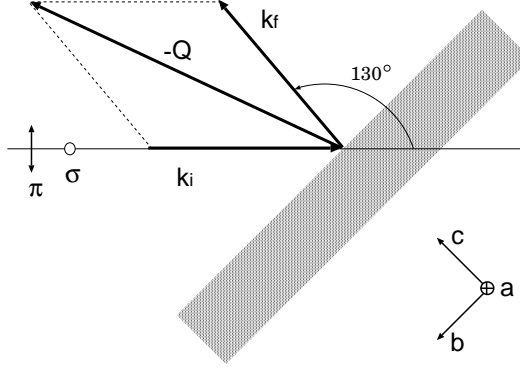


FIG. 4: Schematic view of the scattering geometry. The scattering plane contains the b and c axes. The angle between the incident and scattered x-rays is fixed 130 degrees.

factor, we may confirm from experiment the large contribution of $Y^{(2)}(\omega_i^0; q, \omega)$ in the σ polarization at $q = 3\pi/4$. We also expect to observe the difference in the spectral shapes between in the π and σ polarizations, since the spectral shape of $Y^{(2)}(\omega_i^0; q, \omega)$ has more weights at higher ω than that of $Y^{(1)}(\omega_i^0; q, \omega)$. Within the present finite-size calculation, the spectral peak shifts to a higher energy position in the σ polarization from the position in the π polarization. Although the system of 16 spins may be too small to discuss spectral shapes in detail, the fact that more weights exist at higher ω in $Y^{(2)}(\omega_i; q, \omega)$ than in $Y^{(1)}(\omega_i; q, \omega)$ has been known from the more precise calculation based on the Bethe Ansatz solution,³⁵ if $f_3^{(2)}(\omega_i)$ and $f_4^{(2)}(\omega_i)$ are neglected (actually they are negligible).

IV. CONCLUDING REMARKS

We have studied the magnetic excitations in the L -edge RIXS in one-dimensional undoped cuprates. We have analyzed the second-order dipole allowed process through the intermediate state, in which there is no spin degree of freedom at the core-hole site. This nature of the intermediate state is found to affect strongly the transition amplitudes of spin excitations not only at the core-hole site but also at neighboring sites in the final state. This tendency is found to increase with decreasing values of Γ . The spherical symmetry in the spin space in the ground state makes our analysis transparent, making it possible to analyze the amplitudes giving rise to excitations not only on the core-hole site but also on the neighboring sites. We have evaluated such amplitudes in a finite-size ring. Note that the analysis of the RIXS from the antiferromagnetic ordered state was complicated due to

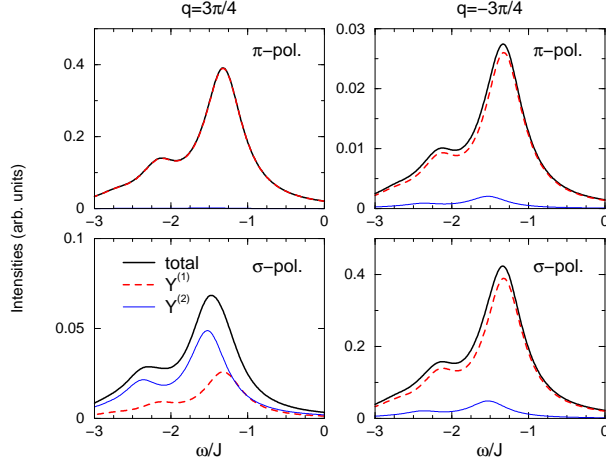


FIG. 5: (Color online) RIXS spectra as a function of energy loss ω for the momentum transfer projected on the b axis $q = 3\pi/4$ and $-3\pi/4$. Black thick solid, red thick broken, and blue thin solid lines are total spectrum, $Y^{(1)}(\omega_i; q, \omega)$, and $Y^{(2)}(\omega_i; q, \omega)$, respectively. The ω_i is set to give rise to the peak in the absorption spectra. $J = 260$ meV and $\Gamma/J = 1.2$. The calculated spectra are convoluted with the Lorentzian function with the half width of half maximum 78 meV.

the presence of the asymmetry in the spin space.²⁸ The RIXS spectra have been expressed as the one-spin correlation function in the channel with changing polarization and as the two-spin correlation function in the channel without changing polarization. We have demonstrated that the contribution of the two-spin correlation function could be observed from the polarization analysis to possible RIXS spectra in Sr_2CuO_3 .

Acknowledgments

We thank Professors M. Grioni and H. M. Rønnow for valuable discussions. This work was partially supported by a Grant-in-Aid for Scientific Research from the Ministry of Education, Culture, Sports, Science and Technology of the Japanese Government.

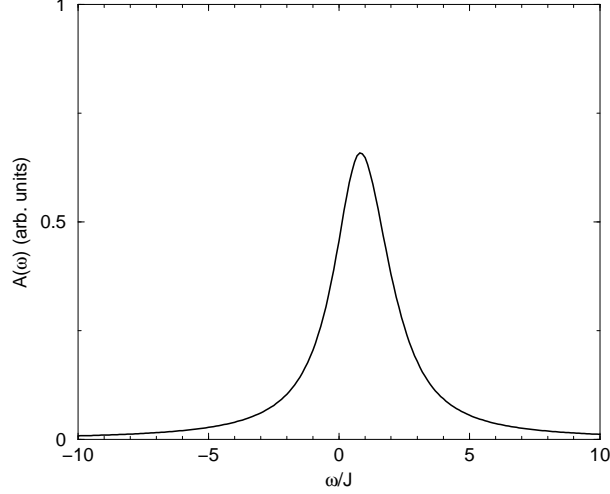


FIG. 6: Absorption coefficient $A(\omega_i)$ as a function of photon energy ω_i . $\Gamma/J = 1.2$. The origin of energy is set to correspond to $\omega_i = \epsilon_{\text{core}}$.

Appendix A: Absorption coefficient

The $L_{2,3}$ -absorption coefficient $A_j(\omega_i)$ ($j = 3/2$ or $j = 1/2$) close to $2p \rightarrow 3d_{x^2-y^2}$ transition may be given by the formula,

$$A_j(\omega_i) \propto \sum_{\sigma, \eta} |\langle \phi_\eta | \psi_0^\sigma \rangle|^2 \frac{\Gamma/\pi}{(\omega_i + \epsilon_g - \epsilon_{\text{core}} - \epsilon'_\eta)^2 + \Gamma^2}. \quad (\text{A1})$$

By substituting the eigenvalues and the eigenstates evaluated on finite-size chain into Eq. (A1), we obtain $A_j(\omega_i)$. Figure 6 shows the calculated $A_j(\omega_i)$ as a function of photon energy. The origin of photon energy is set to be $\omega_i = \epsilon_{\text{core}}$, and $\Gamma/J = 1.2$. The calculated curve is found very close to the Lorentzian shape. The peak position is slightly shifted from $\omega_i = \epsilon_{\text{core}}$; $\omega_i = \omega_i^0 = \epsilon_{\text{core}} + 0.8J$ for $\Gamma/J = 1.2$.

¹ C. -C. Kao, W. A. L. Caliebe, J. B. Hastings, and J. -M. Gillet, Phys. Rev. B **54**, 16361 (1996).

² J. P. Hill, C. -C. Kao, W. A. L. Caliebe, M. Matsubara, A. Kotani, J. L. Peng, and R. L. Greene, Phys. Rev. Lett. **80**, 4967 (1998).

³ M. Z. Hasan, E. D. Isaacs, Z. -X. Shen, L. L. Miller, K. Tsutsui, T. Tohyama, and S. Maekawa, Science **288**, 1811 (2000).

- ⁴ Y. J. Kim, J. P. Hill, C. A. Burns, S. Wakimoto, R. J. Birgeneau, D. Casa, T. Gog, and C. T. Venkataraman, Phys. Rev. Lett. **89**, 177003 (2002).
- ⁵ T. Inami, T. Fukuda, J. Mizuki, S. Ishihara, H. Kondo, H. Nakao, T. Matsumura, K. Hirota, Y. Murakami, S. Maekawa, et al., Phys. Rev. B **67**, 045108 (2003).
- ⁶ Y. J. Kim, J. P. Hill, H. Benthien, F. H. L. Essler, E. Jeckelmann, H. S. Choi, T. W. Noh, N. Motoyama, K. M. Kojima, S. Uchida, et al., Phys. Rev. Lett. **92**, 137402 (2004).
- ⁷ S. Suga, S. Imada, A. Higashiya, A. Shigemoto, S. Kasai, M. Sing, H. Fujiwara, A. Sekiyama, A. Yamasaki, C. Kim, et al., Phys. Rev. B **72**, 081101(R) (2005).
- ⁸ K. Tsutsui, T. Tohyama, and S. Maekawa, Phys. Rev. Lett. **83**, 3705 (1999).
- ⁹ K. Okada and A. Kotani, J. Phys. Soc. Jpn. **75**, 044702 (2006).
- ¹⁰ T. Nomura and J. Igarashi, J. Phys. Soc. Jpn. **73**, 1677 (2004).
- ¹¹ T. Nomura and J. I. Igarashi, Phys. Rev. B **71**, 035110 (2005).
- ¹² J. I. Igarashi, T. Nomura, and M. Takahashi, Phys. Rev. B **74**, 245122 (2006).
- ¹³ J. van den Brink and M. van Veenendaal, Europhys. Lett. **73**, 121 (2006).
- ¹⁴ L. J. P. Ament, F. Forte, and J. van den Brink, Phys. Rev. B **75**, 115118 (2007).
- ¹⁵ L. V. Keldysh, Sov. Phys. JETP **20**, 1018 (1965).
- ¹⁶ M. Takahashi, J. I. Igarashi, and T. Nomura, Phys. Rev. B **75**, 235113 (2007).
- ¹⁷ T. Semba, M. Takahashi, and J. I. Igarashi, Phys. Rev. B **78**, 155111 (2008).
- ¹⁸ J. P. Hill, G. Blumberg, Y. -J. Kim, D. S. Ellis, S. Wakimoto, R. J. Birgeneau, S. Komiya, Y. Ando, B. Liang, R. L. Greene, et al., Phys. Rev. Lett. **100**, 097001 (2008).
- ¹⁹ D. S. Ellis, J. Kim, J. P. Hill, S. Wakimoto, R. J. Birgeneau, Y. Shvyd'ko, D. Casa, T. Gog, K. Ishii, K. Ikeuchi, et al., Phys. Rev. B **81**, 085124 (2010).
- ²⁰ J. van den Brink, arXiv:cond-mat/0510140.
- ²¹ J. van den Brink, Europhys. Lett. **80**, 47003 (2007).
- ²² T. Nagao and J. I. Igarashi, Phys. Rev. B **75**, 214414 (2007).
- ²³ L. Braicovich, L. J. P. Ament, V. Bisogni, F. Forte, C. Aruta, G. Balestrino, N. B. Brookes, G. M. De Luca, P. G. Medaglia, F. M. Granozio, et al., Phys. Rev. Lett. **102**, 167401 (2009).
- ²⁴ L. Braicovich, J. van den Brink, V. Bisogni, M. M. Sala, L. J. P. Ament, N. B. Brookes, G. M. De Luca, M. Salluzzo, T. Schmitt, V. N. Strocov, et al., Phys. Rev. Lett. **104**, 077002 (2010).
- ²⁵ M. Guarise, B. D. Piazza, M. M. Sala, G. Ghiringhelli, L. Braicovich, H. Berger, J. N. Hancock, D. van der Marel, T. Schmitt, V. N. Strocov, et al., Phys. Rev. Lett. **105**, 157006 (2010).

- ²⁶ G. Ghiringhelli, N. B. Brookes, E. Annese, H. Berger, C. Dallera, M. Grioni, L. Perfetti, A. Tagliaferri, and L. Braicovich, Phys. Rev. Lett. **92**, 117406 (2004).
- ²⁷ L. J. P. Ament, G. Ghiringhelli, M. M. Sala, L. Braicovich, and J. van den Brink, Phys. Rev. Lett. **103**, 117003 (2009).
- ²⁸ J. Igarashi and T. Nagao, arXiv:1104.4683.
- ²⁹ J. I. Igarashi and T. Nagao, Phys. Rev. B **72**, 014403 (2005).
- ³⁰ M. W. Haverkort, Phys. Rev. Lett. **105**, 167404 (2010).
- ³¹ J. P. Hannon, G. T. Trammell, M. Blume, and D. Gibbs, Phys. Rev. Lett. **61**, 1245 (1988).
- ³² F. Forte, M. Cuoco, C. Noce, and J. van den Brink, Phys. Rev. B **83**, 245133 (2011).
- ³³ L. Hulthen, Arkiv. Mat. Astron. Fysik **38**, 1 (1938).
- ³⁴ J. des Cloizeaux and J. J. Pearson, Phys. Rev. **128**, 2131 (1962).
- ³⁵ A. Klauser, J. Mossel, J.-S. Caux, and J. van den Brink, Phys. Rev. Lett. **106**, 157205 (2011).